Supporting Information

Construction of Fe-Ni Energy Bridge for NIR-II Luminescence Enhancement and Anti-Thermal Quenching via Microwave-Induced Defect Engineering

Xiaomeng Wang [a], Jiaren Du *[a], Dariusz Hreniak [b], Wiesław Stręk [b] Kai Jiang [a] and Hengwei Lin *[a]

[a] *International Joint Research Center for Photo-responsive Molecules and Materials, School of Chemical and Material Engineering, Jiangnan University*

214122, Wuxi, China E-mail: jiaren.du@jiangnan.edu.cn linhengwei@jiangnan.edu.cn

[b] *Division of Optical Spectroscopy, Institute of Low Temperature and Structure Research, Polish Academy of Sciences, Okólna 2, Wrocław 50-422, Poland*

Supplementary Methods

Materials Preparation

The NIR-II phosphor samples

The Ca_2ScSbO_6: Fe^{3+}, Ni^{2+} (CSSO: Fe^{3+}, Ni^{2+}) was prepared by traditional solid-state reaction (SSR). The starting materials, $CaCO_3$ (99.9%, Macklin), Sc_2O_3 (99.99%, Aladdin), NiO (99.95%, Aladdin) and Sb_2O_3 (99.95%, Aladdin), were weighed according to stoichiometric ratios. The precursors were sintered in air at 1500 °C in a muffle furnace for 6 hours with the heating rate of 5◦C min^{-1}. The sample was then cooled down to room temperature in furnace, and the obtained powder was fully ground for further analysis.

The Microwave-induced treatment (MWIT) samples

The 0.8 g sample of CSSO: Fe^{3+}, Ni^{2+} prepared by SSR were weighed for further microwave treatment. The home-built microwave reaction device was composed of two alumina crucibles and

aluminum silicate insulation bricks. The larger crucible (50 mL) holds the activated carbon (200 mush, Leyan), while the smaller crucible (5 mL) contains 0.8 g of the precursor. The smaller crucible was covered with an alumina tray and inserted into the activated carbon within the larger crucible. The inner and smaller crucible was tightly covered with an alumina disk to hold the reaction temperature and prevent contact with the volatilized carbon. There are 8 g of activated carbon in the larger crucible. The two crucibles are then placed into the cavity of a high-temperature aluminosilicate insulation brick. The materials were irradiated in a lab microwave oven (frequency: 2.45 GHz) for 20 minutes with a microwave power of 700 W. The obtained powder was fully ground for further analysis.

Structural and Morphological Characterization

The crystallographic phase purity of the obtained phosphors was examined by X-ray diffraction (XRD) using an X-ray powder diffractometer (D8, Bruker AXS GmbH, Germany) with Cu Kα1 (1.5406 Å) radiation (40 kV, 40 mA) at room temperature. The oxygen vacancies were measured by the X-ray photoelectron spectroscopy (XPS) using the X-ray photoelectron spectrometer equipped with Al Kα rays (Thermo Scientific Nexsa, USA), the beam spot is 300 um, vacuum degree of the analysis chamber is better than $3.0E^{-7}$mBar, the Operating voltage and Filament current is 12 kV and 6 mA. The electron paramagnetic resonance (EPR) data was collected using the desktop electron paramagnetic resonance spectrometer with the microwave power of 10 mW (ESR 5000, Bruker, Germany). The morphology of samples prepared using the four different synthesis methods was characterized using scanning electron microscope (SEM) and the morphology of samples synthesized using the SSR and MWIT was analyzed using SEM (S4800, Hitachi, Japan), The elemental analysis of CSSO: Fe^{3+}, Ni^{2+} prepared by SSR and MWIT were characterized using energy dispersive spectrometer (EDS) equipped on SEM (Regulus 8100, Hitachi, Japan).

Luminescence Characterization

The room-temperature steady-state photoluminescence (PL), photoluminescence excitation (PLE) spectra, and luminescence decay profiles were measured by a fluorescence spectrometer (FLS1000, Edinburgh, UK) with a monochromated 450 W Xenon arc lamp as the excitation source. The diffuse reflection spectra (DRS) were obtained by a UV–vis spectrophotometer

(SHIMADZU UV-2700, Japan) with $BaSO_4$ used as the reference standard. The images of all patterns were taken using Vision Camera (Canon EOS Rebel T5i) and SWIR Camera (LD-SW640171550, Xi'an Leading Optoelectronic Tech. CO., LTD, China).

NIR pc-LED fabrication.

The CSSO: Fe^{3+}, Ni^{2+} phosphors were ground to obtain the fine and homogenous powders. The prepared CSSO: Fe^{3+}, Ni^{2+} phosphors were dispersed in epoxy resin (A:B = 2:1) to form a composite solution. The NIR pc-LED device was fabricated by precoating the composite solution onto a 365 nm UV chip and dried at 50 °C for 1 h. The optical performances of the as-fabricated NIR-II pc-LED were measured with a home-built testing system. The direct current ranging from 20 to 500 mA were obtained by the programmable power supply (IT-M7700, ITECH, USA), the luminescent spectra were measured by the NIRQuest+1.7 900-1700 nm equipped with the ISP-50-8-I 50MM integrating sphere. (Ocean optics, USA). The real-time temperature was measured by the Fluke infrared imager (Ti480 Pro, Fluke, USA).

Table S1. Lattice parameter of CSSO:Fe^{3+}, Ni^{2+}

a (Å)	b (Å)	c (Å)	Alpha	Beta	Gamma	Volume (Å^3)
5.513369	5.637029	7.865996	90	90.0278	90	244.467

Table S2. Lattice parameter of MWIT-CSSO:Fe^{3+}, Ni^{2+}

a (Å)	b (Å)	c (Å)	Alpha	Beta	Gamma	Volume (Å^3)
5.501111	5.629268	7.853716	90	89.9989	90	243.208

Table S3. Atomic occupation of CSSO:Fe^{3+}, Ni^{2+}

label	x	y	z
Ca1	0.006	0.0446	0.2477
Sb1	0	0.5	0
Sc1	0.5	0	0
O1	0.334517	0.300014	0.065411
O2	0.26637	0.293201	0.456795
O3	0.872003	0.485497	0.23186

Table S4. Atomic occupation of MWIT-CSSO:Fe^{3+}, Ni^{2+}

label	x	y	z
Ca1	0.015	0.0461	0.249
Sb1	0	0.5	0
Sc1	0.5	0	0
O1	0.292	0.303	0.052
O2	0.299	0.284	0.444
O3	0.908	0.468	0.244

Table S5. Parameters of the emission wavelength (λ_{em}) and thermal quenching ratio ($I_{High\ Temp}/I_{293K}$) for phosphors doped with Fe^{3+} ions.

Material	λ_{em} (nm)	Thermal quenching ratio ($I_{High\ Temp}/I_{293K}$) @ High Temp.(K)	References
$CaLaMgSbO_6:Fe^{3+}$	990	42%@373K	1
$NaScSi_2O_6:Fe^{3+}$	900	23%@423K	2
$SrMgAl_{10}O_{17}:Fe^{3+}$	808	69.1%@423K	3
$KAl_{11}O_{17}:Fe^{3+}$	770	95%@423K	4
$RbAl_{11}O_{17}:Fe^{3+}$	770	75%@423K	4
$Li_2ZnSiO_4:Fe^{3+}$	750	35.3%@373K	5
$LiAlO_2:Fe^{3+}$	725	55.3%@413K	6
$ZnGa_2O_4:Fe^{3+}$	720	72%@423K	7
$Ca_2ScSbO_6:Fe^{3+}$, Ni^{2+}	960	103%@423K	This work

Table S6. Parameters of the emission wavelength (λ_{em}) and thermal quenching ratio ($I_{High\ Temp}/I_{293K}$) for phosphors doped with Ni^{2+} ions.

Material	λ_{em} (nm)	Thermal quenching ratio ($I_{High\ Temp}/I_{293K}$) @ High Temp.(K)	References
Ba_2MgWO_6:Ni^{2+}	1630	50%@423K	8
$Ca_3Ga_2Ge_3O_{12}$: Cr^{3+}，Ni^{2+}	1490	50%@375K	9
$Mg_3Ga_2GeO_8$: Ni^{2+}	1490	56%@373K	10
$Gd_3Mg_{0.5}Al_{1.5}Ga_{2.5}Ge_{0.5}O_{12}$: Cr^{3+}, Yb^{3+}, Ni^{2+}	1480	39.6%@423K	11
$Ca_3Al_2Ge_3O_{12}$: Cr^{3+}, Ni^{2+}	1423	52.4%@423K	12
$LiMgPO_4$: Cr^{3+}, Ni^{2+}	1380	57%@393K	13
$MgTa_2O_6$: Ni^{2+}	1290	5%@393K	14
$MgGa_2O_4$: Cr^{3+}, Ni^{2+}	1260	67%@423K	15
$LiGa_5O_8$: Cr^{3+}, Ni^{2+}	1232	60%@410K	16
$LiAlSiO_4$:Cr^{3+}, Ni^{2+}	1150	25%@423K	17
Ca_2ScSbO_6: Fe^{3+}, Ni^{2+}	1560	65%@423K	This work

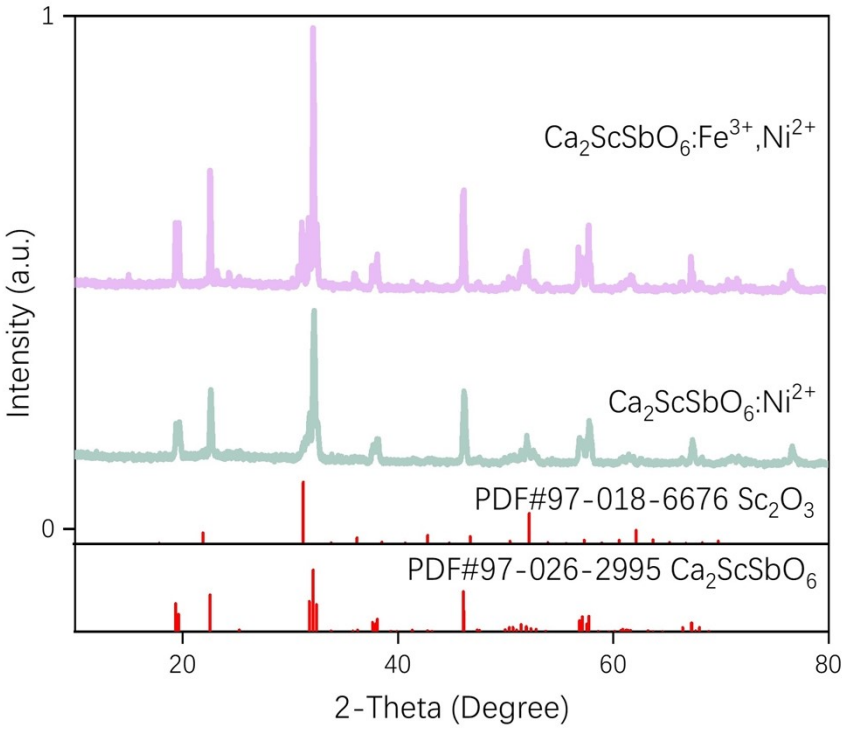

Figure S1. The XRD of CSSO: Fe^{3+}, Ni^{2+} and CSSO: Ni^{2+}.

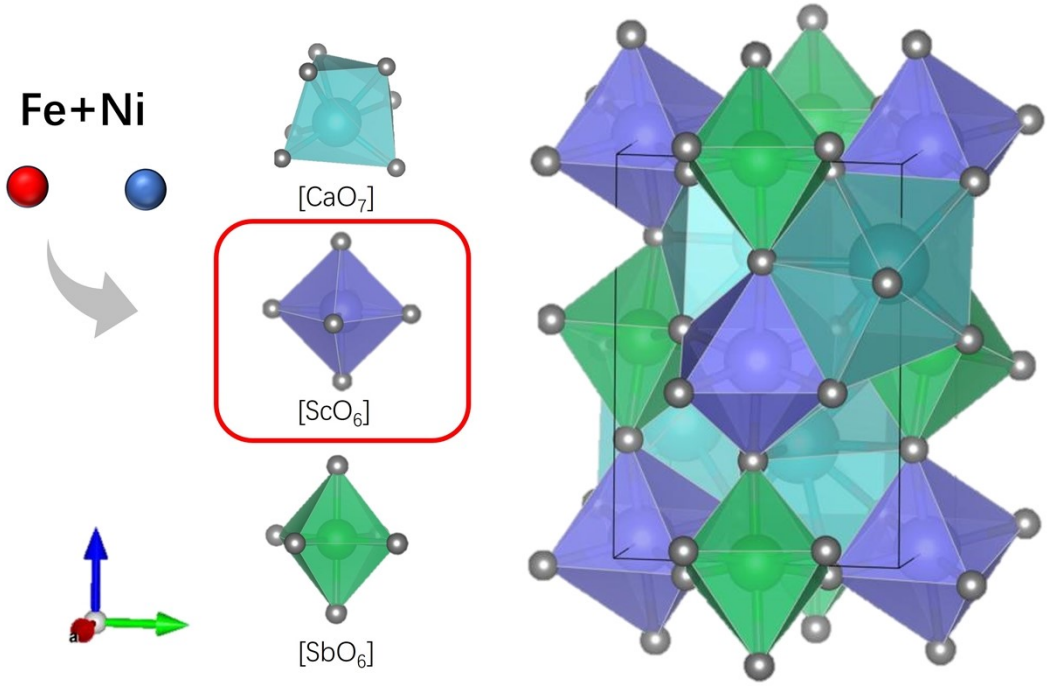

Figure S2. The crystal structure of CSSO: Fe^{3+}, Ni^{2+}.

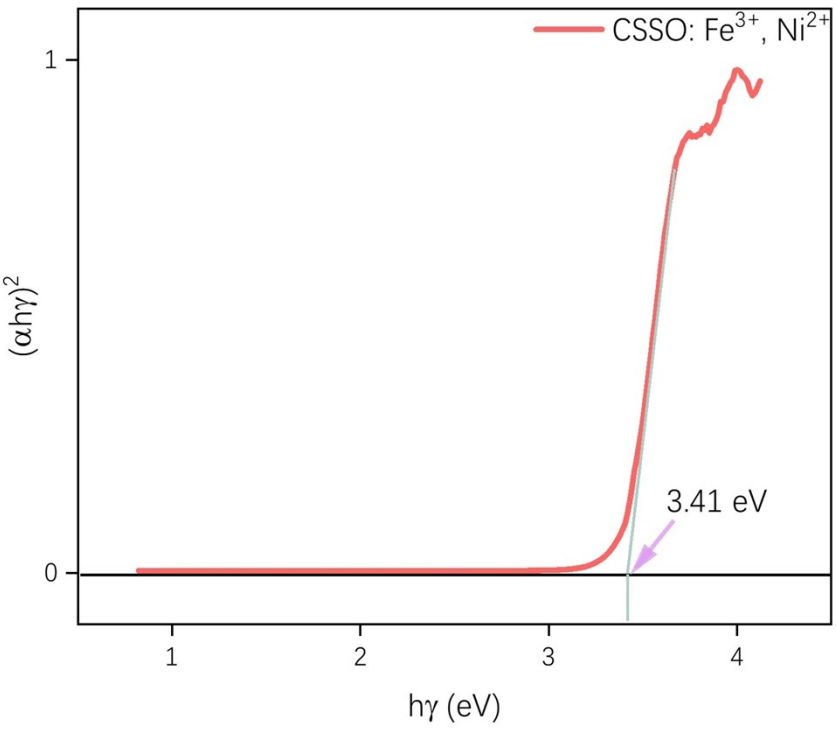

Figure S3. The plot of absorption coefficient against photon energy for CSSO: Fe^{3+}, Ni^{2+}.

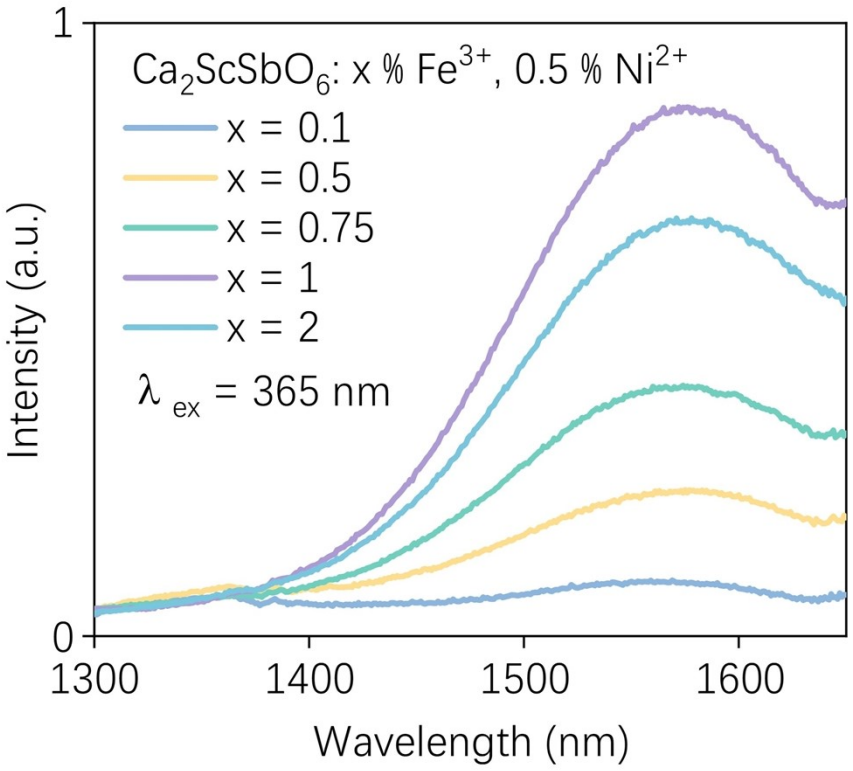

Figure S4. The PL (λ_{ex} = 365 nm) of the Ca_2ScSbO_6: x% Fe^{3+}, 0.5% Ni^{2+} (x = 0.1, 0.5, 0.75, 1, 2).

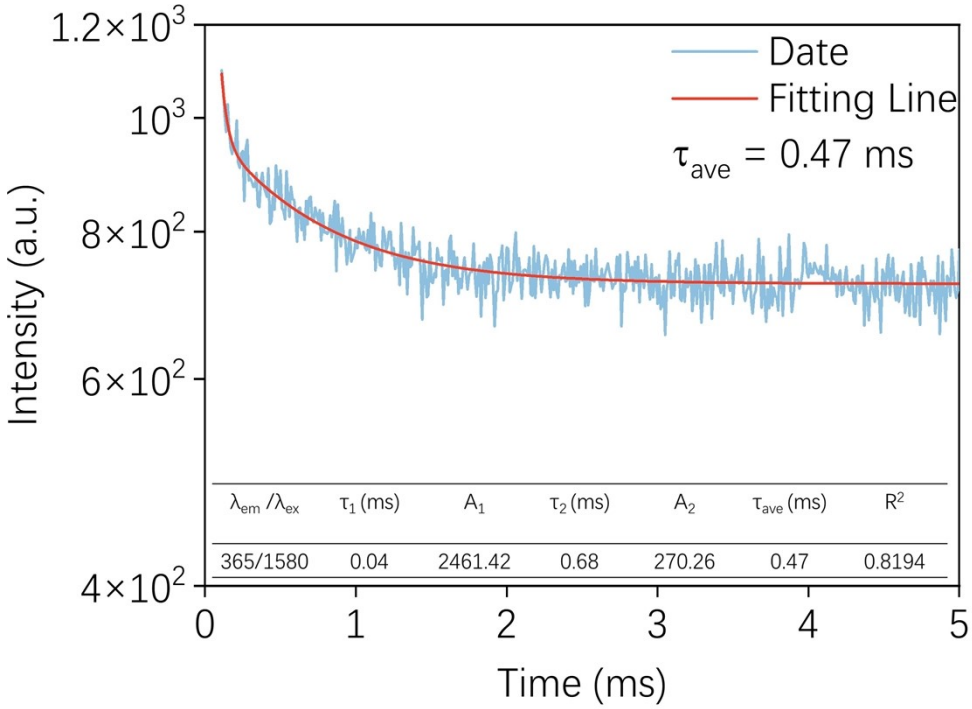

Figure S5. The average lifetime of CSSO: Ni^{2+} (λ_{ex} = 365 nm, λ_{em} = 1580 nm).

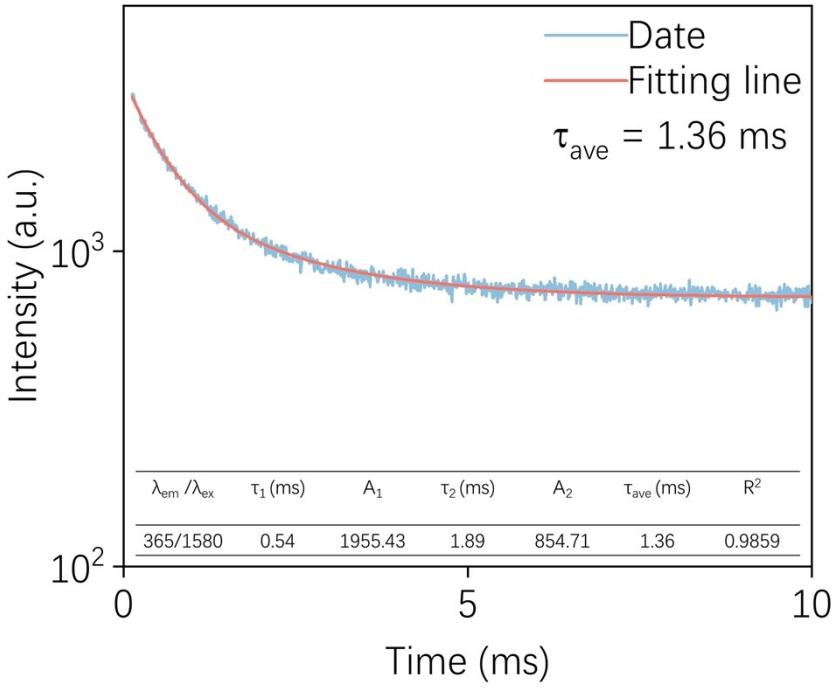

Figure S6. The PL decay curve of CSSO:Fe^{3+}, Ni^{2+} (λ_{ex} = 365 nm, λ_{em} = 1580 nm).

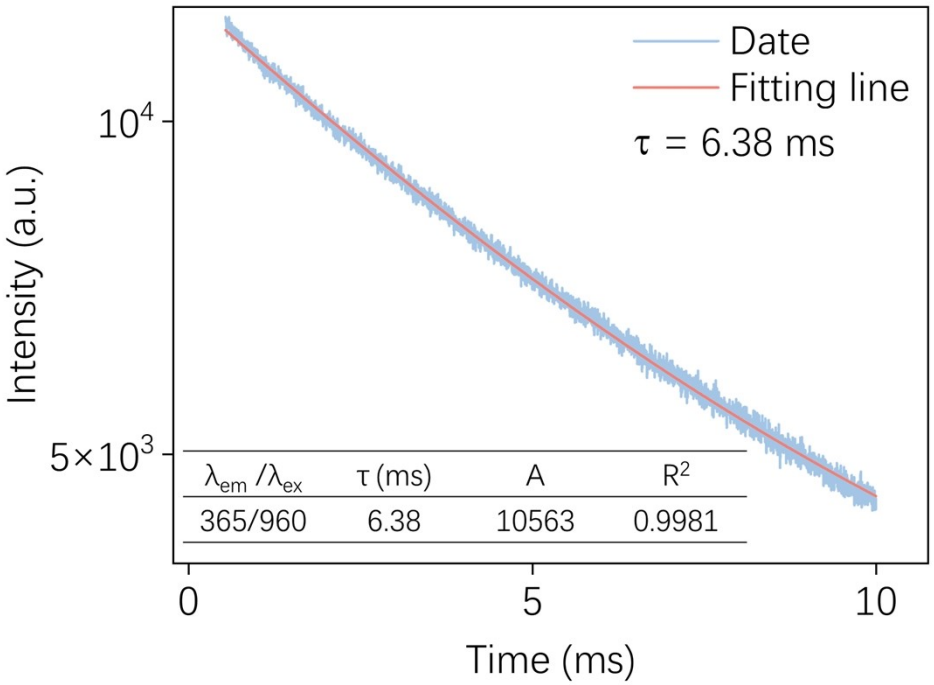

Figure S7. The PL decay curve of CSSO:Fe^{3+} (λ_{ex} = 365 nm, λ_{em} = 960 nm).

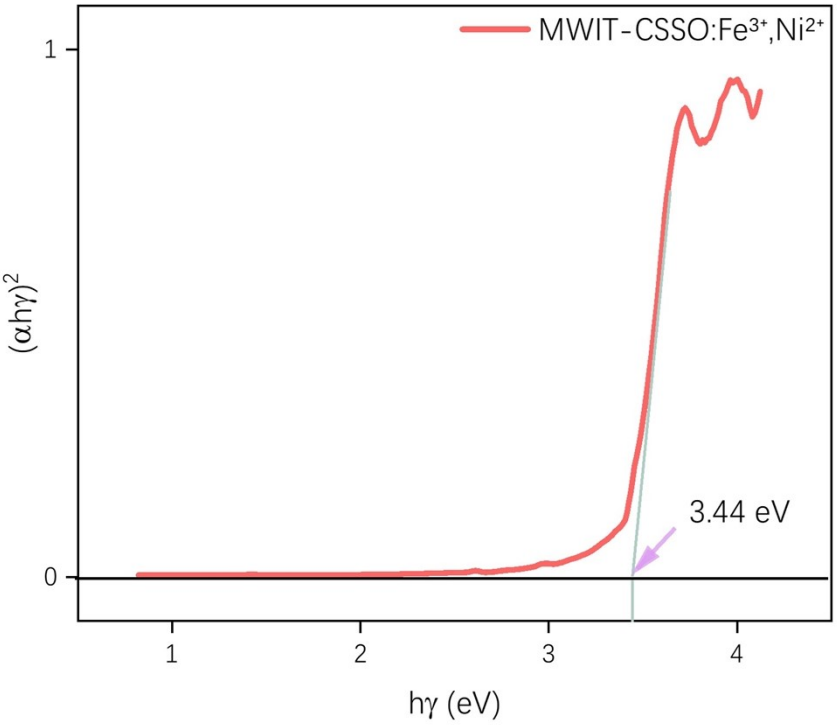

Figure S8. The plot of absorption coefficient against photon energy for MWIT-CSSO:Fe^{3+}, Ni^{2+}.

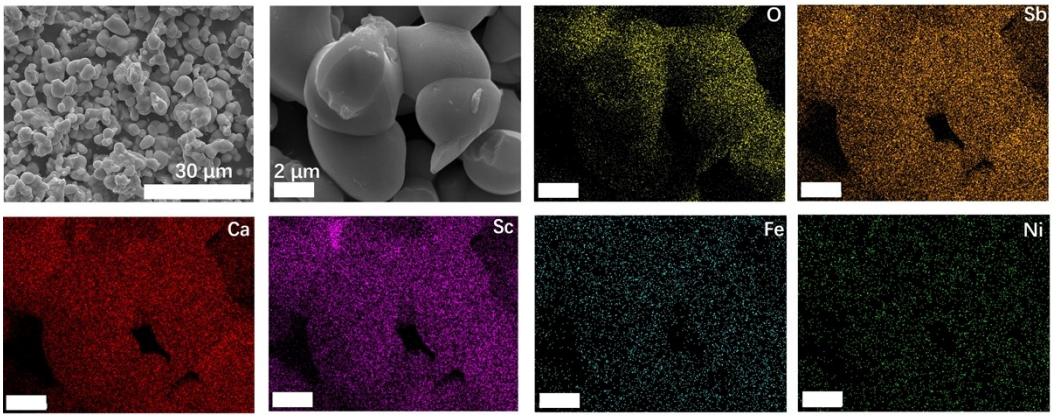

Figure S9. SEM images and EDS elemental mappings of CSSO:Fe^{3+}, Ni^{2+}.

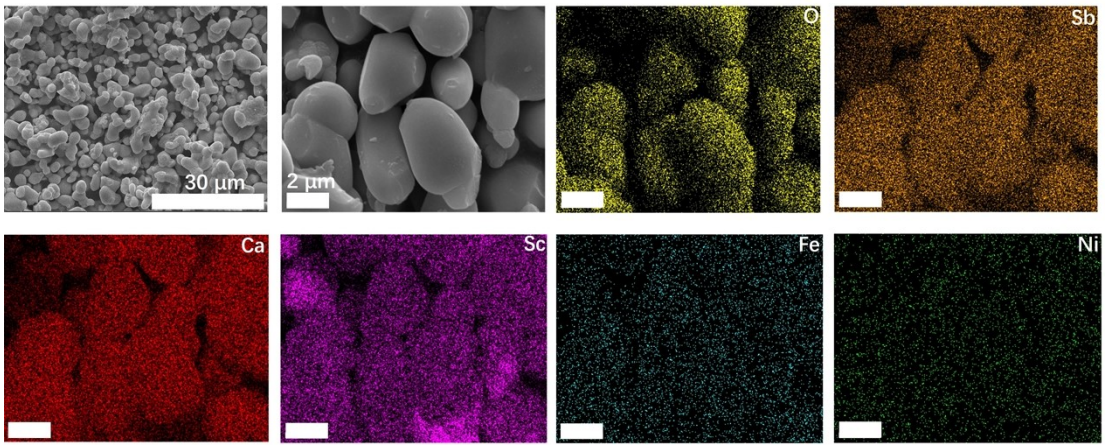

Figure S10. SEM images and EDS elemental mappings of MWIT-CSSO:Fe^{3+}, Ni^{2+}.

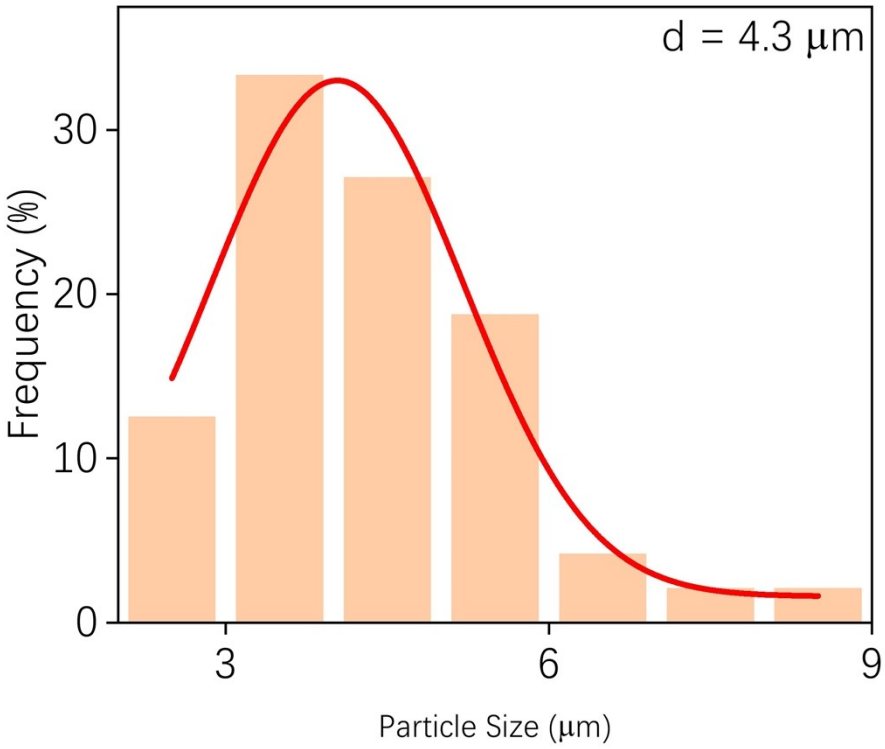

Figure S11. Analysis of particle size distributions accompanied by corresponding fitting curves of the CSSO:Fe^{3+}, Ni^{2+}.

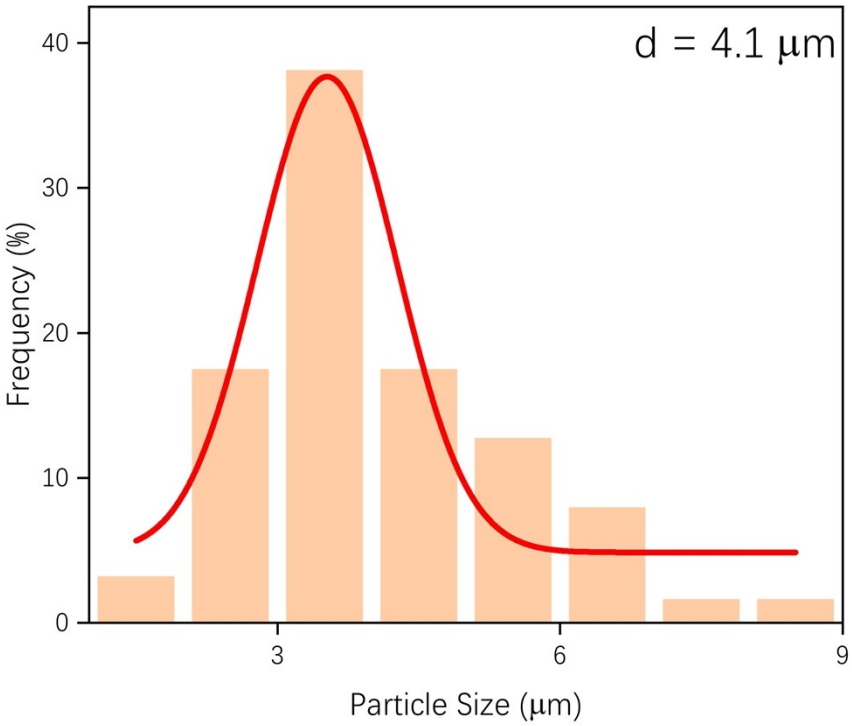

Figure S12. Analysis of particle size distributions accompanied by corresponding fitting curves of the MWIT-CSSO:Fe^{3+}, Ni^{2+}.

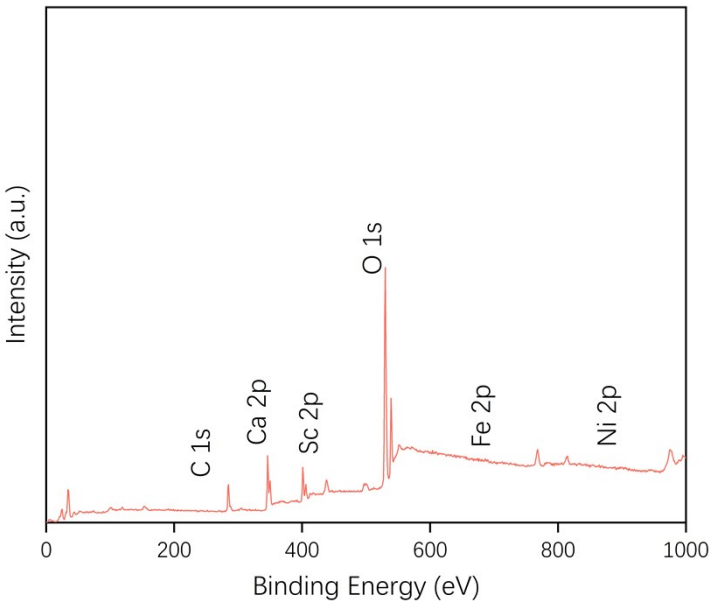

Figure S13. The XPS survey of CSSO:Fe^{3+}, Ni^{2+}.

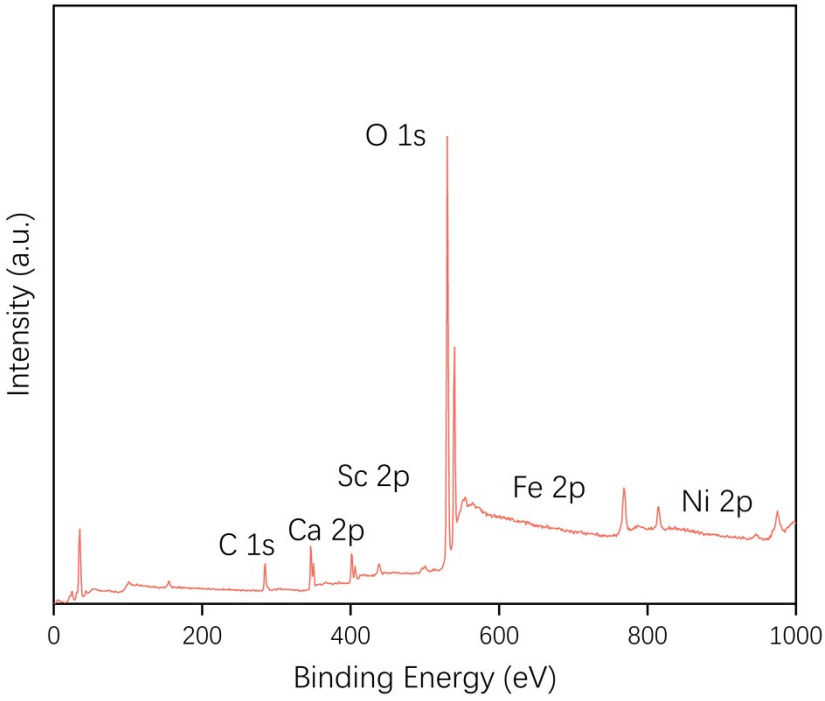

Figure S14. The XPS survey of MWIT-CSSO:Fe^{3+}, Ni^{2+}.

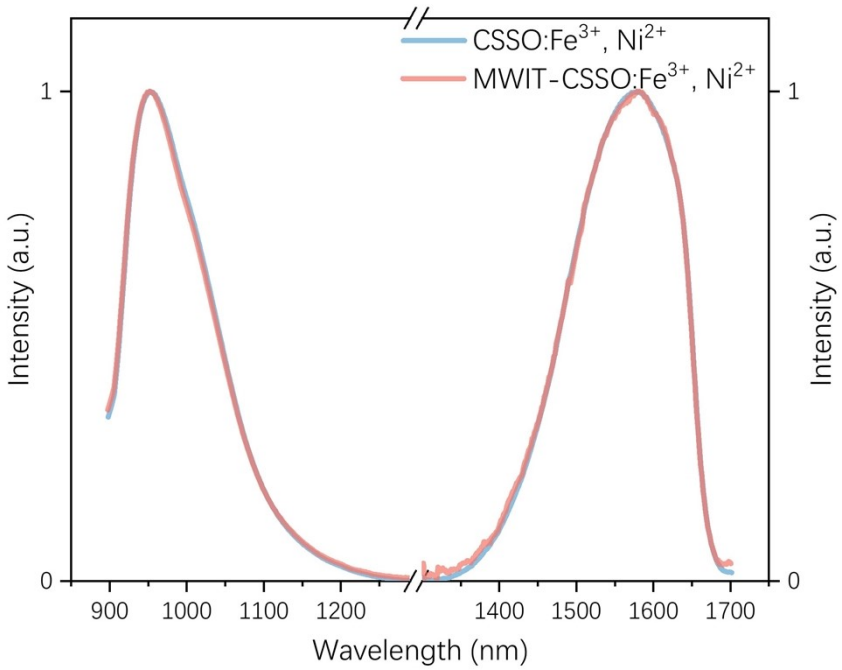

Figure S15. The PL spectra (λ_{ex} = 365 nm) of CSSO:Fe^{3+}, Ni^{2+} and MWIT-CSSO:Fe^{3+}, Ni^{2+}.

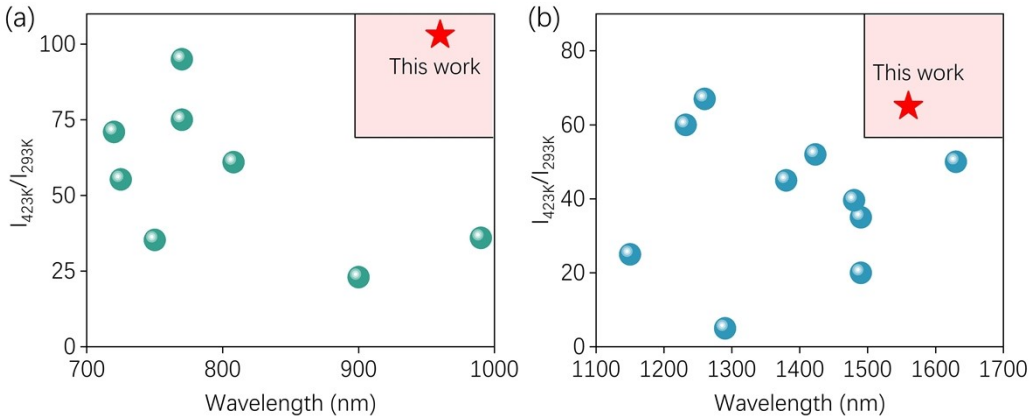

Figure S16. Parameters of the emission wavelength (λ_{em}) and thermal quenching ratio ((I_{423K}/I_{293K}) for phosphors incorporating (a) Fe^{3+} ions and (b) Ni^{2+} ions.

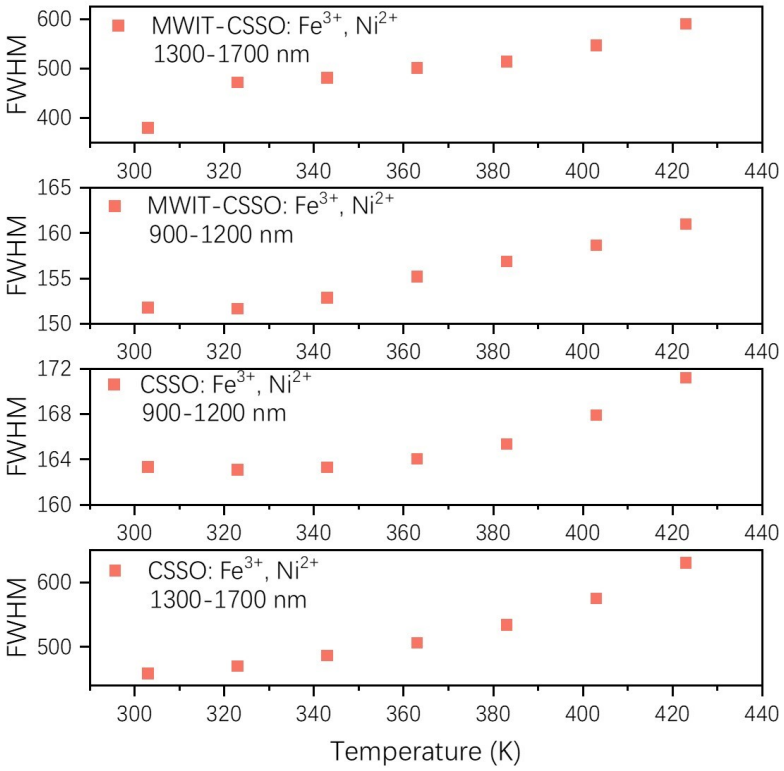

Figure S17. The FWHM of CSSO:Fe^{3+}, Ni^{2+} and MWIT-CSSO:Fe^{3+}, Ni^{2+} with the increase of temperature.

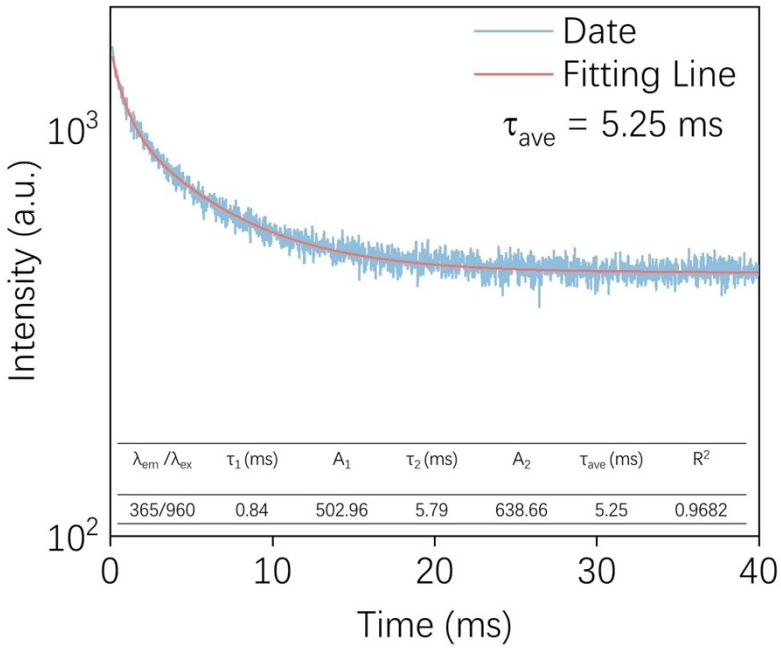

Figure S18. The PL decay spectra of CSSO:Fe^{3+},Ni^{2+} with λ_{ex} = 365 nm and λ_{em} = 960 nm.

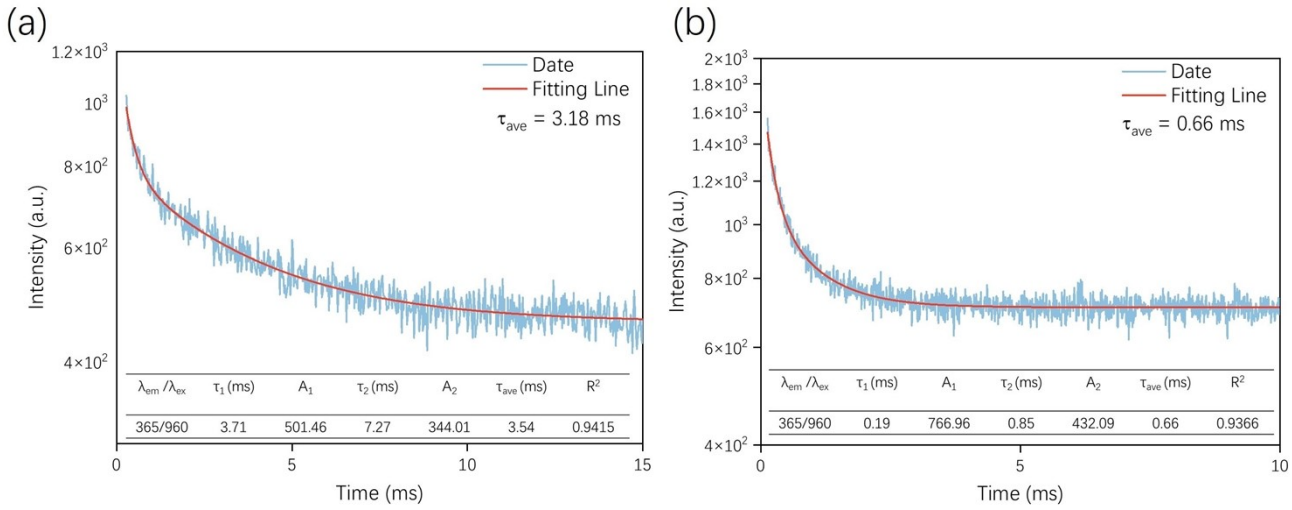

Figure S19. The PL decay spectra of MWIT-CSSO:Fe^{3+},Ni^{2+} with (a) λ_{ex} = 365 nm and λ_{em} = 960 nm, (b) λ_{ex} = 365 nm and λ_{em} = 1580 nm.

References

1. S. Su, C. Hu, S. Ding, Y. Sun, L. Sun, Y. Zou, R. Liu, Z. Lei, B. Teng and D. Zhong, *Adv. Opt. Mater.*, 2023, **12**, 2302383.
2. X. Zhang, D. Chen, X. Chen, C. Zhou, P. Chen, Q. Pang and L. Zhou, *Dalton Trans.*, 2022, **51**, 14243-14249.
3. R. Cao, J. Bai, J. Nie, F. Cheng, B. Lan, L. Zhang, J. Duan and J. Wang, *J. Alloy. Compd.*, 2025, **1021**, 179639.
4. J. Ni, Y. Chen, B. Qu and L. Wang, *Optical Materials: X*, 2022, **16**, 100212.
5. Y. Yang, L. Shen, J. Zhang, S. Zhao, Q. Pang, X. Zhang, P. Chen and L. Zhou, *Inorg. Chem.*, 2023, **62**, 12862-12871.
6. K. Cheng, X. Liu, Q. Lu, D. Wu, W. Huang and C. Deng, *Spectrochim. Acta A*, 2024, **308**, 123784.
7. L. Xiang, X. Zhou, Y. Wang, L. Li, S. Jiang, G. Xiang, C. Jing, J. Li and L. Yao, *J. Lumin.*, 2022, **252**, 119293.
8. X. Lu, Y. Gao, J. Chen, M. Tan and J. Qiu, *ACS Appl. Mater. Interfaces.*, 2023, **15**, 39472-39479.
9. F. Zhao, Y. Shao, Q. Liu and J. Zhong, *Laser Photonics Rev.*, 2024, **18**, 2400447.
10. C. Wang, J. Lin, X. Zhang, H. Dong, M. Wen, S. Zhao, S. Yuan, D. Zhu, F. Wu and Z. Mu, *J. Alloy. Compd.*, 2023, **942**, 168893.
11. L. Jiang, L. Zhang, X. Jiang, J. Xie, G. Lv and Y. Su, *Adv. Mater. Technol*, 2023, **9**, 2301495.
12. B.-M. Liu, X.-X. Guo, L.-Y. Cao, L. Huang, R. Zou, Z. Zhou and J. Wang, *Chem. Eng. J.*, 2023, **452**, 139313.
13. S. Miao, Y. Liang, Y. Zhang, D. Chen and X. J. Wang, *Adv. Mater. Technol*, 2022, **7**, 2200320.
14. F. Zhu, Y. Gao, B. Zhu, L. Huang and J. Qiu, *Chem. Eng. J.*, 2024, **479**, 147568.
15. S. Miao, Y. Liang, R. Shi, W. Wang, Y. Li and X.-J. Wang, *ACS Appl. Mater.*, 2023, **15**, 32580-32588.
16. S. Liu, Y. Guo, M. Zhao, J. Du, Z. Song, X. Zhang, F. Wang and Q. Liu, *Laser Photonics Rev.*, 2024, **18**, 2400475.
17. Y. Li, Y. Lu, H. Ju, W. Wang, D. Tu, H. Lu, J. Wang and H. Zou, *ACS Appl. Opt. Mater.*, 2024, **2**, 1933-1938.